Journal of Statistical Physics (2021) 184:7
https://doi.org/10.1007/s10955-021-02779-1

Local Violation of Conservation in the Abelian Sandpile Model Through Fractal Patterns of Non-conservative Sites

L. Elyasizad[1] · M. D. Niry[1,2]

Received: 9 December 2019 / Accepted: 15 May 2021 / Published online: 28 June 2021

Abstract
In this paper we investigate the two-dimensional Abelian sandpile model in which the conservation of sand grains is locally violated using non-conservative lattice sites. We use spatially correlated arbitrary fractal patterns to mark the non-conservative sites. We have observed a "crossover" in the scaling behavior of the distribution functions of both the avalanche areas and avalanche sizes. The pre-crossover scaling exponents are known already and are related to the embedding dimension of the model. In addition to these, we have found that new "post-crossover" scaling exponents result from fractality. In fact we have found a spectrum of values for these exponents across the fractal dimensions $1 \leq d_f \leq 2$ with a dominantly declining "linear" trend.

Keywords Self-organized criticality · Abelian sandpile model · Fractal patterns · Scaling exponents

1 Introduction

In contrast to the traditionally well-known critical systems such as those, for example, described by the Ising model where the fine-tuning of the temperature is necessary to approach criticality, many natural phenomena display scale-free (power-law) behavior, which is the main feature of a critical state and they do this without any external tuning of the parameters. This spontaneous approach to the critical state is the so called Self-Organized Criticality (SOC) [1–3]; a non-equilibrium phenomenon that occurs in nonlinear systems with infinitesimally small inputs. For a linear system in the equilibrium state, a small perturbation will cause a small disturbance. This means that the response of the system is proportional to the

Communicated by Eric A. Carlen.

✉ M. D. Niry
m.d.niry@iasbs.ac.ir
http://www.iasbs.ac.ir/~m.d.niry/

1 Department of Physics, Institute for Advanced Studies in Basic Sciences (IASBS), Zanjan 45137-66731, Iran

2 Center for Research in Climate Change and Global Warming (CRCC), Institute for Advanced Studies in Basic Sciences (IASBS), Zanjan 45137-66731, Iran

size of the perturbations. On the other hand, in a self-organized critical system, the system's response to an external perturbation might be anything from a simple small reaction to a cascade of reactions called an avalanche [2].

The most well-known model that illustrates SOC is the BTW sandpile model introduced by Bak, Tang and Wiesenfeld in 1987 [4]. For simplicity, we use a subclass of the model with the particular properties of Abelian group, known as the Abelian sandpile model which was introduced by Dhar in 1990 [5]. The essential point in an SOC model is the preservation of the conservation law for a fluctuating variable [6]. Therefore the crucial point in the sandpile model is the conservation of the sand grains in such a way that at each time step the number of the sand grains is conserved 'inside' the lattice. The sand grains, however, are allowed to leave the system at the boundaries. Tsuchiya *et al.* showed that the BTW model fails to be critical when a slight annihilation is introduced in the toppling process 'inside' the lattice, in addition to its boundaries (*i.e.*, bulk dissipation) [7]. Manna *et al.* violated conservation locally by creating and annihilating sand grains locally, but on average, the number of the sand grains was conserved. They showed that the local violation of conservation did not destroy criticality but the scaling exponents of their system did not belong to the same universality class as the normal BTW model [6]. Moghimi-Araghi *et al.* also violated conservation locally through quenched and annealed randomness. They labeled some sites as sinks that would dissipate sand grains and labeled some other sites as sources that would produce sand grains [8]. We use a similar model and call those sites non-conservative in the rest of this paper.

In some studies deterministic fractal patterns are used as the lattice in the usual BTW model [9]. But, up till now in the non-conservative sandpile models, the non-conservative sites do not have any specific spatial patterns (*i.e.*, they are uncorrelated). In the model that we consider, we construct the non-conservative sites by drawing them from fractal patterns with an arbitrary Hausdorff dimension d_{f} between 1 and 2 inclusively (*i.e.*, $1 \leq d_{\mathrm{f}} \leq 2$) [10]. At each time step they could be identified as a sink or a source with equal probability as explained in Ref. [8]. Investigating the probability distribution function of the avalanche sizes shows a crossover in the power-law behavior resulting in two different scaling exponents. Both exponents are slowly related to the fraction of the non-conservative sites p [11]. Also, the post-crossover exponent seems to be dependent on the fractal dimensions of the patterns.

From statistical mechanics we know that the critical exponents are independent from the details of interactions and the structure of the lattice (e.g., the coordinate number), but they depend on the embedding dimensions. Our results indicate that the self-similarity of the patterns of non-conservative sites and the fractal dimensions characterizing them affect the critical exponents. The rest of the manuscript is organized as follows. In the next section our non-conservative sandpile model is introduced and then the generation of the fractal patterns is explained. Section 3 is dedicated to the results and discussions, and the summary and conclusion are presented in the last section.

2 Methods

Our method is divided into two parts. In Sect. 2.2, we show how to generate two-dimensional binary (square) patterns of $\{s_{ij}\}$ that are used to mark the non-conservative sites. These inhomogeneous patterns are fractals with long-range correlation. As will be discussed, we define $s_{ij} = 1$ as the non-conservative case and define p as the ratio of the number of non-conservative sites to the total number of sites. In this way, we produce patterns with

arbitrary fractal dimensions and different values of p. Then, we apply these patterns to our non-conservative model introduced below.

2.1 The Non-conservative Abelian Sandpile Model

We consider the usual Abelian sandpile model on an $L \times L$ square lattice where L is chosen in powers of 2 in the range 2^7 to 2^{10} to improve the efficiency of our algorithm and optimal distribution of data on a logarithmic scale. For each site (i, j), we define z_{ij} which takes discrete values of 1 to 4. At each time step, we perturb a randomly chosen site (i, j) by changing the corresponding z_{ij} to $z_{ij} + 1$. z_{ij} may exceed the threshold value of $z_c = 4$ in which case the site becomes unstable and topples [5]. For the non-conservative model the toppling rule is

$$\begin{cases} z_{ij} & \to z_{ij} - z_c, \\ z_{i'j'} & \to z_{i'j'} + 1 + \xi_{i'j'}, \quad (i', j') \in \text{n.n.}(i, j) \end{cases} \tag{1}$$

where n.n.(i, j) is a set of pairs denoting the nearest neighbors of the site (i, j). For a conservative site (i, j), $\xi_{i'j'} = 0$. But if the site (i, j) is non-conservative, at each toppling, for one of the nearest neighbors that is chosen randomly, the corresponding $\xi_{i'j'}$ is $+1$ or -1 with equal probability and for the rest of the nearest neighbors, $\xi_{i'j'} = 0$. As a result, if the site is non-conservative it will topple just like the conservative one except that in one of its nearest neighbors, which is randomly chosen, a grain of sand will be dissipated or produced with equal probability. Transferring sand grains according to the toppling rule [Eq. (1)] may make other sites unstable so that they may topple and a chain of topplings called 'avalanche' is probable.

As was previously mentioned, the patterns of the non-conservative sites are spatially correlated so that they illustrate fractal patterns. In the following section, we use the modified Fourier filtering method to produce fractal patterns with arbitrary fractal dimensions [12].

2.2 Generating the Two-Dimensional Binary Patterns with Long-Range Correlation

We aim to generate two-dimensional binary patterns of $s_{ij} = 0, 1$ which have long-range correlation. Therefore the correlation function

$$C(r) = \langle s_{ij} s_{i'j'} \rangle \big|_{r^2=(i-i')^2+(j-j')^2}, \tag{2}$$

follows the scaling rule $(1 + r^2)^{-\gamma/2}$ where γ is the correlation exponent. We define $s_{ij} = 1$ as a non-conservative site and $s_{ij} = 0$ as a conservative site.

To do this, we used the modified Fourier filtering method in two-dimension introduced in detail by Makse *et al.* in Ref. [12]. This method enables us to produce two-dimensional patterns with long-range correlation.

After producing correlated patterns the next step is applying the Heaviside step function with different threshold values to find the binary patterns and then calculating the fraction of non-conservative sites, p. However applying the thresholds almost changes the fractal dimension of the patterns and the correlation exponents. So we recalculate the Hausdorff dimension applying the well-known box-counting method [10] (The ImageJ software, Ver. 1.x was used [13]). Since some samples are small ($128 \leq L \leq 2048$), and some of them are inhomogeneous, the fractal dimension is estimated by the correlation dimension method to verify the results [14]. Figure 1d shows the consistency of both the box-counting and the correlation dimension with errors of about ± 0.05. There are many types of dimensions

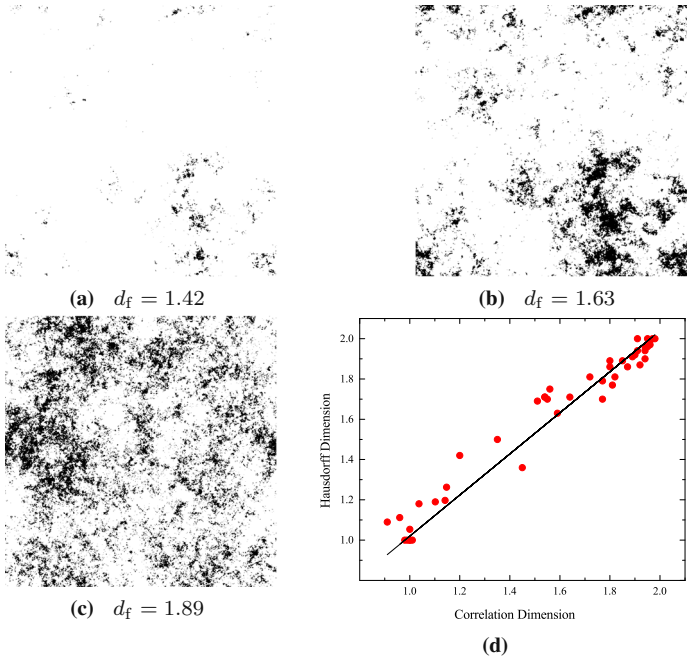

Fig. 1 Binary 1024×1024 patterns with arbitrary fractal dimensions and different values of p, **a** $p = 1\%$, **b** $p = 10\%$, and **c** $p = 20\%$. The dark pixels represent the non-conservative sites. **d** The scatter plot of the Hausdorff dimension of samples estimated by the box-counting method *vs.* the correlation dimension. The solid line drawn through the data points has a slope of 1, as a guidance

for fractal sets, and it is not clear which should be involved in our problem. Also, there are different methods to estimate each of them, but we chose the box-counting method to estimate the Hausdorff dimension since it is simple and fits the data adequately. By the way, applying the modified Fourier filtering method and different thresholds enables us to generate random binary patterns with arbitrary fractal dimensions ($d_f \gtrsim 1.3$) and different values of $p > 0.5‰$ (e.g., see Fig. 1).

Also, we applied the one-dimensional modified Fourier filtering method to produce a fractal curve [12]. This curve was plotted on a two-dimensional mesh to produce a pattern with $1 < d_f < 1.2$; see Fig. 2a. In addition to fractal patterns, some regular patterns with integer dimensions $d_f = 1, 2$ were also used in our investigation. See Fig. 2b, c for samples. Finally, to ensure that the results do not depend on the method we used to generate the self-similar patterns, we added several random fractal patterns, such as those shown in Fig. 2d–f, to our collection.

3 Results and Discussion

Our investigation shows that the implemented non-conservative model is still critical and displays scaling behavior but there is a crossover in the distribution function of the characteristic properties of the avalanches. Therefore two different exponents are obtained. For example, Fig. 3a shows the distribution of avalanche sizes. The crossover at $s_\times$ in the distribution function is marked with a vertical dashed line. For avalanches smaller than $s_\times$, the power-law

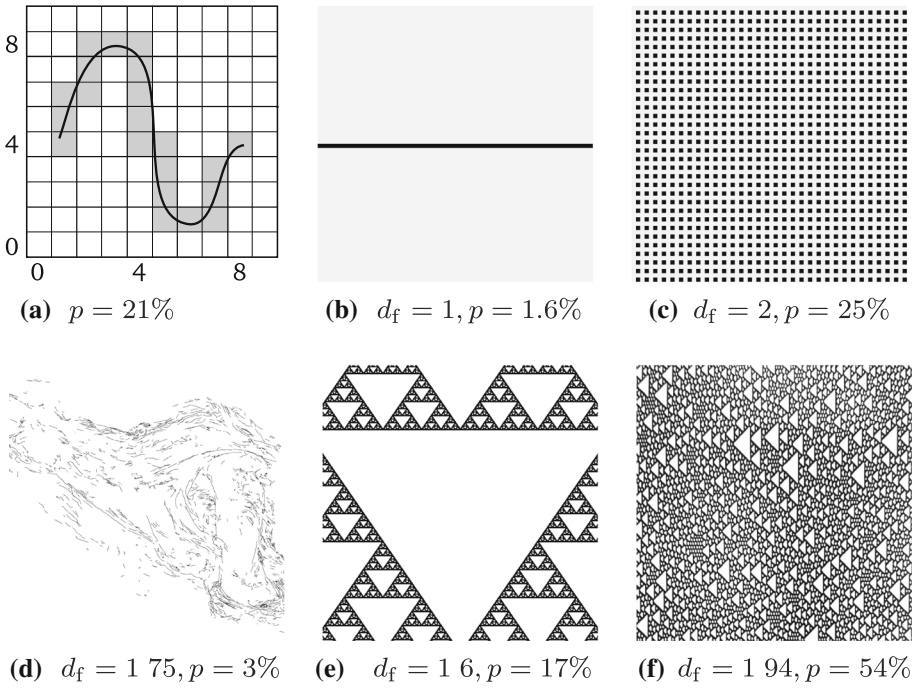

(a) $p = 21\%$ **(b)** $d_{\mathrm{f}} = 1, p = 1.6\%$ **(c)** $d_{\mathrm{f}} = 2, p = 25\%$

(d) $d_{\mathrm{f}} = 1\ 75, p = 3\%$ **(e)** $d_{\mathrm{f}} = 1\ 6, p = 17\%$ **(f)** $d_{\mathrm{f}} = 1\ 94, p = 54\%$

Fig. 2 **a** A typical curve plotted on a two-dimensional 10×10 lattice to produce a binary pattern, **b** a solid line with a specific thickness, **c** a checkerboard, **d** a stochastic fractal of the Iranian plateau's faults, **e** the Sierpinski triangle, and **f** a random Sierpinski carpet

behavior is characterized by ν_1 and for $s > s_\times$ a new power-law behavior with the scaling exponent ν_2 appears. ν_2 is obtained using a linear fit to the log-log plot of the distribution, excluding the crossover region (*i.e.*, $s \lesssim s_\times$) and the tail of the distribution function [see Fig. 3a]. The error in the tail is caused by the lack of large avalanches, due to the finite size of the lattice.

In small avalanches (*i.e.*, $s < s_\times$), an avalanche might spread without seeing any non-conservative sites and would not be influenced by the spatial distribution of those sites (*i.e.*, their fractality). So in this regime, our system behaves just like the usual conservative sandpile model with a finite lattice. In the sandpile model, the exponents associated with the avalanche sizes (τ_{s}) slowly relate to the system size [15] as,

$$\tau_{\mathrm{s}}(L) = \tau_{\mathrm{s}}(\infty) - \frac{c}{\ln L}. \tag{3}$$

Moghimi-Araghi *et al.* have shown that although the bulk dissipation rate is averagely zero, the fraction of the non-conservative sites p in the system affects τ_{s} similar to the system size. In addition to dissipation in the boundaries, the model also has dissipation/production at the non-conservative sites. So we have another length scale which is $1/\sqrt{p}$, if the non-conservative sites are homogeneously distributed over the lattice. This length scale might have the same effect on the dynamics of the system as L [8,16]. So by substituting $l \sim 1/\sqrt{p}$ by L in Eq. (3) we have

$$\nu_1(p) = \nu_1(0) + c'/\ln p, \tag{4}$$

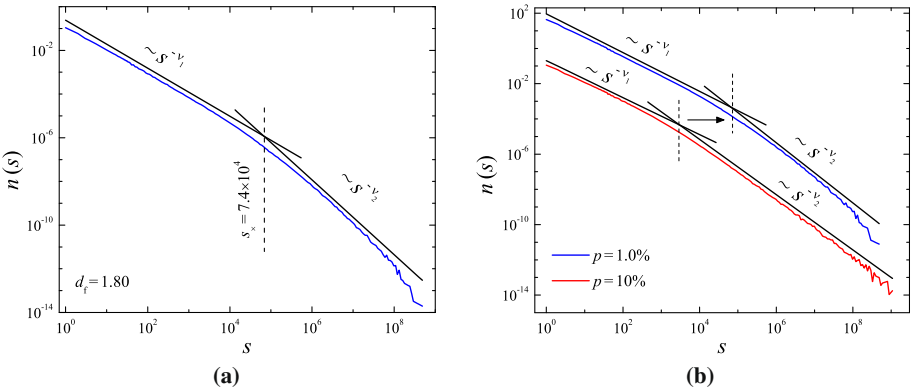

Fig. 3 The log-log plot of the distribution function $n(s)$ for avalanches of size s in a 1024×1024 lattice. Solid lines show a linear fit to the corresponding region of the curves excluding the crossover. The vertical dashed lines show the crossover, $s_\times$. **a** A specific pattern of non-conservative sites with fractal dimension $d_f = 1.80$ and $p = 1\%$. $\nu_1 = 1.10 \pm 0.02$ shows the exponent of the fit for avalanches with $s < s_\times$ and $\nu_2 = 1.71 \pm 0.02$ is the exponent for $s > s_\times$. **b** Two different patterns with different values of p. For clarity, the curve corresponding to $p = 1\%$ has been shifted up. $s_\times$ experiences a shift from 2.9×10^3 to a higher value of 7.4×10^4 as p decreases

for the small length scale, which is verified in Ref. [16]. Investigating the distribution function of the avalanche sizes shows that the pre-crossover exponent ν_1 decreases gradually as p is increased and this agrees with previous results [8,16].

In fact, the existence of two different exponents indicates that there are two different regimes involved. In the first regime, where the sizes of the avalanches are small, the non-conservative sites are not involved in the toppling process and our model behaves like the usual Abelian sandpile model. But in the second regime where $s > s_\times$, the avalanches spread over the non-conservative sites and the power-law behavior is influenced by them, so the new scaling exponent ν_2 appears at the tail of the distribution function. Figure 3b shows that as p increases $s_\times$ decreases. For large values of p, the participation of the non-conservative sites in the toppling process is more probable, so they might be involved in avalanches with smaller sizes compared to the case where the values of p are low. Results show that ν_2 might be related to d_f (see Fig. 4). Since there are large avalanches ($s > s_\times$) that might spread all over the system and reach the boundaries, they would be affected by both of the characteristic length scales l and L. So we expect that ν_2 is a function of d_f, p, and L.

We should figure out the ν_2 dependence on L and p and eliminate their effects on our results. Considering Eq. (3), we know that the dependence on L vanishes at infinite size. Also we can see in Eq. (4) that for small values of p the dependence on p may be negligible. So we expect that for the samples with $p < 1\%$ and $L \geq 1024$ illustrated with the empty circles in Fig. 4, the effects of p and L on ν_2 are negligible. The solid line in Fig. 4 shows the trend in ν_2 for these samples. If we successfully eliminate the effects of p and L on ν_2, all results may render the same trend. We assume that the ν_2 dependence on L and p may be separated into

$$\nu_2(d_f, p, L) = \nu_2(d_f, 0, \infty) + f(d_f, p) + g(d_f, L), \tag{5}$$

where $f(d_f, p)$ vanishes at infinitesimal p and $g(d_f, L)$ vanishes at infinite L. Considering Eqs. (3) and (4), we guess that the logarithms of p and L would affect our results and Eq. (5)

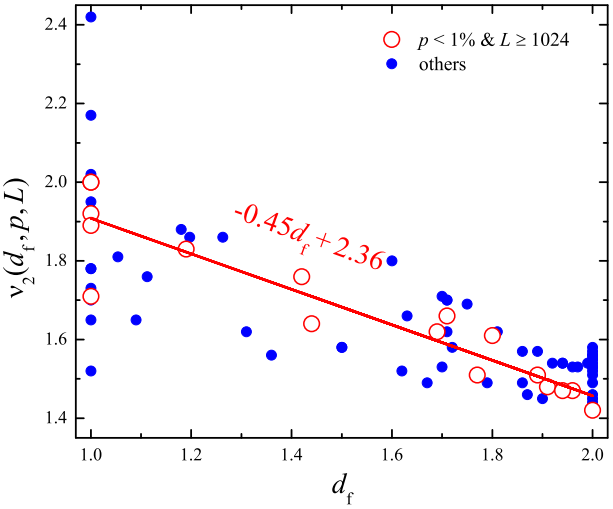

Fig. 4 ν_2 is plotted against d_f for different values of p and L. The empty circles (○) show the samples with $L \geq 1024$ and $p \lesssim 1\%$, in which the dependence of ν_2 on p and L is rather small. The solid line shows a linear fit to the empty circles. The solid circles (●) show other samples that are scattered from the linear fit due to the effects of p and L

can be rewritten as,

$$\nu_2(d_f, p, L) = \nu_2(d_f, 0, \infty) + \frac{(p-1)c_1(d_f)}{\log p} + \frac{c_2(d_f)}{\log L}, \tag{6}$$

where c_1 and c_2 are coefficients that depend on d_f. Considering that Eq. (4) has a singularity at $p = 1$, we have replaced its second term with $(p-1)/\log p$, which is well-defined at $p = 1$. We will show that this simple correction, in addition to solving the problem of the singularity at $p = 1$, predicts the behavior of the critical exponents close to the singular point (see ▼ symbols in Fig. 5). However, we will discuss later that the case $p \sim 1$ in the thermodynamic limit is only meaningful for $d_f = 2$. Finally, it should be noted, the correction form of p as $(p-1)/\log p$ in Eq. (6) is inspired by the correction form $1/\log L$ for the system size. According to our numerical results, it seems our assumption is plausible.

In order to find $c_1(d_f)$ we restrict d_f and L to fixed values so that the variations of ν_2 are only caused by the variations of the second term in Eq. (6). Then c_1 can be determined to be a constant. In Fig. 5 the slope of the solid lines shows c_1 for $d_f = 1$ and 2. We repeat this approach to find c_1 for different values of d_f. The results are presented in Fig. 6. To clarify the variations of p in this figure the logarithmic scale is used for the x-axis. The solid curves represent linear fits of ν_2 against $(p-1)/\log p$. As $\nu_2(p) \sim c_1(p-1)/\log p$, their slope represents c_1 for the corresponding d_f. The inset in Fig. 6 shows c_1 as a function of d_f. A similar method can be used to obtain $c_2(d_f)$ except that we look at the variations in ν_2 while keeping the values of d_f and p fixed. Finally the coefficients are obtained as

$$c_1(d_f) \approx 2.72 - 1.32 d_f, \tag{7a}$$

$$c_2(d_f) \approx -3.65 + 1.69 d_f. \tag{7b}$$

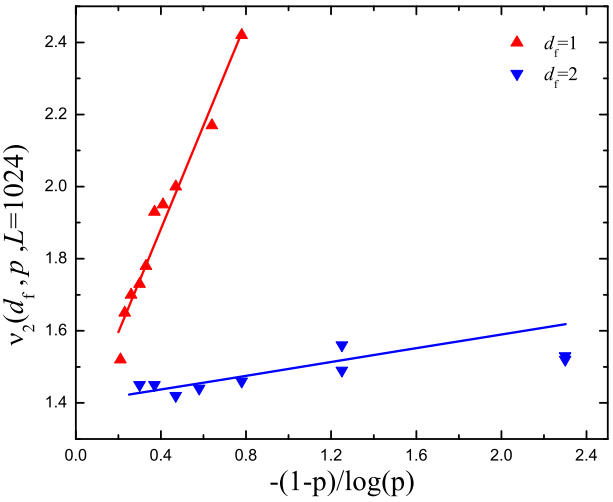

Fig. 5 ν_2 is plotted *versus* $(p-1)/\log p$. The term $1-p$ resolves the singularity at $p=1$. Furthermore corrects the behavior of the exponent for large values. L and d_f are fixed at specific values. The slope of the solid lines denotes c_1 for the corresponding d_f

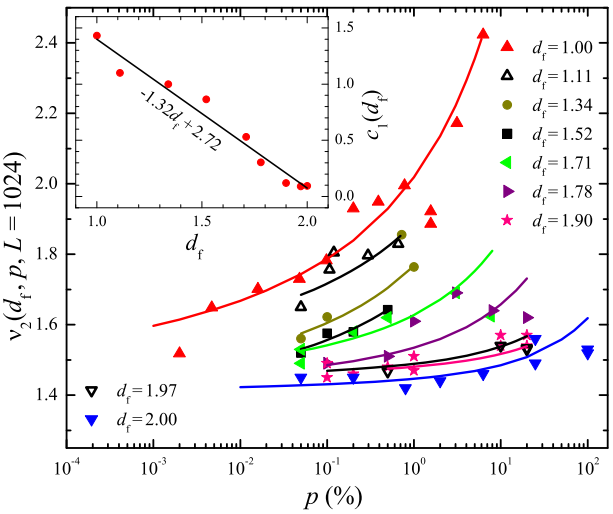

Fig. 6 ν_2 for $L=1024$ is plotted against p. The solid curves represent linear fits of ν_2 *versus* $(p-1)/\log p$. The inset shows the slope of these linear fits (c_1) *vs.* d_f. As the solid line in the inset shows, $c_1(d_f) = 2.72 - 1.32 d_f$

By substituting Eqs. (7a) and (7b) in Eq. (6), we obtain $\nu_2(d_f, 0, \infty)$. The results show that $\nu_2(d_f, 0, \infty)$ depends linearly on d_f as

$$\nu_2(d_f, 0, \infty) \approx 2.36 - 0.43 d_f. \tag{8}$$

Equations (7a) and (7b) are linear and now Eq. (8) is also linear, therefore we can use the multidimensional least squares method to find all the 6 parameters simultaneously [*i.e.*, the three pairs of slopes and intercepts in Eqs. (7) and (8)], as explained in chapter 9 of Ref. [17]:

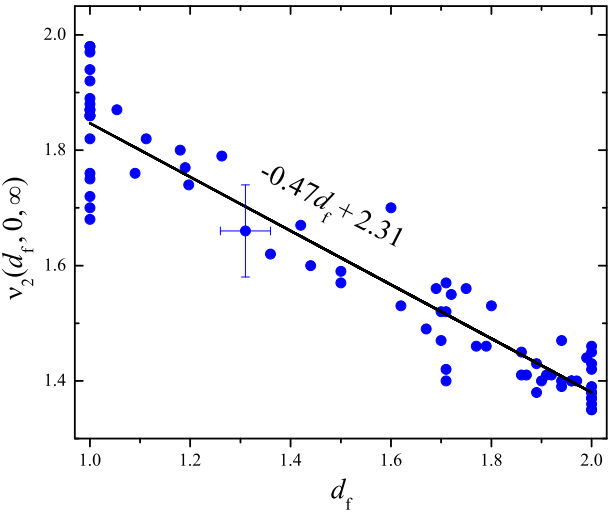

Fig. 7 A plot of the scaling exponent ν_2 of the patterns of sites with different fractal dimensions d_f; the exponent is corrected according to Eq. (6). The single error bars denote the average error of obtaining d_f and ν_2 for all samples. The solid line shows a linear fit to the data rendering $\nu_2(d_f, 0, \infty) = -0.47d_f + 2.31$ which shows a trend similar to the one in Fig. 4

$$c_1(d_f) = 2.34 - 1.14d_f, \tag{9a}$$

$$c_2(d_f) = -3.06 + 1.59d_f, \tag{9b}$$

$$\nu_2(d_f) = 2.31 - 0.47d_f. \tag{9c}$$

This method slightly improved our previous results. We obtained $\nu_2(d_f, 0, \infty)$ explicitly as illustrated in Fig. 7. The data points with $d_f = 1$ are scattered due to the fact that for small values of p the post-crossover regions in $n(s)$ are small, so the error of obtaining ν_2 is high.

Just like the avalanche sizes, avalanche areas also render a crossover in the distribution function (see Fig. 8). A vertical dashed line denotes the crossover at $a_\times$. For avalanches smaller than $a_\times$, μ_1 characterizes the scaling behavior and for $a > a_\times \approx \pi l^2$, a new scaling behavior with the scaling exponent μ_2 appears. Figure 9 shows $\mu_2(d_f, p, L)$ for different patterns. Because of the finite size of the system, there is a limit to the area of an avalanche. It cannot be larger than the area of the system, L^2. As a result the new scaling region characterized by μ_2 is small, and the error of obtaining the exponent is higher than the error in determining ν_2. We discarded some data where the deviation is too large. The new scaling region is large enough only for large values of p. In such cases we have to eliminate the effect of p. But due to the lack of data (Fig. 9), performing the elimination and obtaining $\mu_2(d_f, 0, \infty)$ is not simple.

We assume that $\mu_2(d_f, p, L)$ is a function of d_f, p, and L in the same form as $\nu_2(d_f, p, L)$:

$$\mu_2(d_f, p, L) = \mu_2(d_f, 0, \infty) + \frac{(p-1)b_1(d_f)}{\log p} + \frac{b_2(d_f)}{\log L}, \tag{10}$$

$\mu_2(d_f, 0, \infty)$, $b_1(d_f)$, and $b_2(d_f)$ depend linearly on d_f. According to Eq. (10), we expect that for infinitesimal p and infinite L, 2nd and 3rd terms are negligible [For details, see the explanation below Eq. (6)]. The empty circles in Fig. 9, show the samples with $p < 1\%$ and

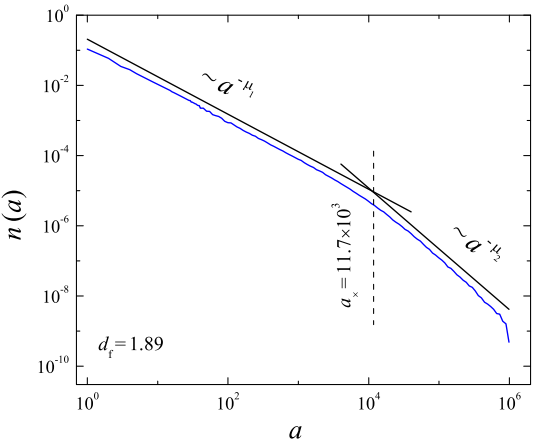

Fig. 8 The log-log plot of the distribution function $n(a)$ for avalanches of area a in a 1024×1024 lattice. Solid lines show linear fits to the corresponding regions of the curves and the vertical dashed line shows the crossover $a_\times$. A specific pattern of non-conservative sites with the fractal dimension of $d_f = 1.89$ and $p = 1\%$ is used. $\mu_1 = 1.09 \pm 0.02$ and $\mu_2 = 1.47 \pm 0.03$ show the pre- and post-crossover exponents

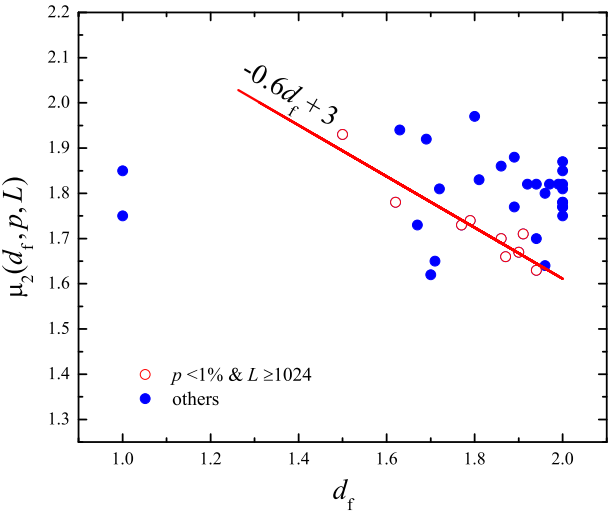

Fig. 9 μ_2 is plotted against d_f for patterns with different values of p and L. The empty circles (○) show the samples with $p \lesssim 1\%$ and $L \geq 1024$ in which the dependency on the other parameters is irrelevant. The solid line shows a linear fit to the empty circles. The solid circles (●) show μ_2 for other samples scattered away from the solid line due to the effects of other parameters (*i.e.*, p and L)

$L \geq 1024$. So according to Eq. (10), for these samples $\mu_2(d_f, p, L) \approx \mu_2(d_f, 0, \infty)$. The solid line shows the linear trend in these samples. We expect that after successful elimination of the effects of p and L from $\mu_2(d_f, p, L)$, the whole data in Fig. 9 will converge to the linear trend $\mu_2(d_f, 0, \infty)$.

As the multidimensional least squares method improved our results in obtaining $\nu_2(d_f, 0, \infty)$, we applied it to determine $\mu_2(d_f, 0, \infty)$. Then all the 6 parameters are obtained as:

$$b_1(d_f) = 0.76 - 0.35d_f, \tag{11a}$$

$$b_2(d_f) = -3.05 + 1.63d_f, \tag{11b}$$

$$\mu_2(d_f) = 3 - 0.6d_f. \tag{11c}$$

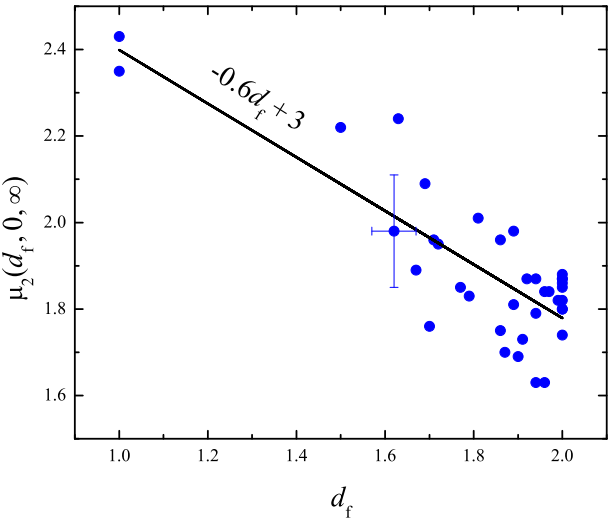

Fig. 10 A plot of the scaling exponent μ_2 of patterns with different fractal dimensions d_f; the exponent is corrected as $\mu_2(d_f, 0, \infty)$ according to Eq. (10). The single error bars denote the average error of obtaining d_f and ν_2 for all samples. The solid line shows the linear trend in $\mu_2(d_f, 0, \infty)$ as $-0.6d_f + 3$

Now by substituting Eqs. (11) in Eq. (10) we are able to obtain $\mu_2(d_f, 0, \infty)$ as illustrated in Fig. 10.

4 Summary and Conclusion

Investigation of the distribution function of the avalanche size (area) showed that a crossover occurs in the scaling behavior resulting in two different scaling exponents obtained on both sides of the crossover region denoted by $s_\times$ ($a_\times$). We found that $s_\times$ and $a_\times$ are related to the fraction of the non-conservative sites p, and so are the exponents ν_1 and μ_1. The scaling behavior presented in Eq. (4) is discussed in Ref. [16]. We figured out that the exponents of the second regime (ν_2 and μ_2) depend on the Hausdorff dimensions of the patterns used in the model, as shown in Figs. 4 and 9. Meanwhile we found that these new exponents also depend on the two different length scales l and L, where l shows the average distance between non-conservative sites and depends on p. We studied the dependence of the exponents on p and L and eliminated their effects on our results [see Eqs. (6) and (10) and the discussion that follows]. For many patterns with specific values of d_f, p and L, the scaling exponents $\nu_2(d_f, p, L)$ and $\mu_2(d_f, p, L)$ were obtained, and then our elimination method was used to obtain the corresponding exponents $\nu_2(d_f, 0, \infty)$ and $\mu_2(d_f, 0, \infty)$. Taking into account the error in determining the exponents, Figs. 7 and 10 show that all of the exponents obtained show a clear (declining) linear trend as a function of d_f. As our results are derived from numerical simulations, we could find out only the leading term, which is linear. It seems, our method more or less succeeded to eliminate the effects caused by p and L. Although in the case of the avalanche 'areas', because of the lack of data, the error in obtaining $\mu_2(d_f, 0, \infty)$ is higher than that of $\nu_2(d_f, 0, \infty)$.

The number of non-conservative sites (denoting the mass of a fractal pattern) is proportional to L^{d_f}. So the fraction of the non-conservative sites is $p \sim L^{d_f - 2}$. For infinite sizes

and $0 \leq d_f < 2$, p will tend to zero. The special case of non-zero p is only possible for $d_f = 2$, and in this case, which has already been investigated [8], the critical exponents in the thermodynamic limit depend on p in addition to d_f [see Eqs. (6) and (10)].

The small length scale $l = p^{-\frac{1}{2}} \sim L^{1-d_f/2}$. As L goes to infinity, l will tend to infinity too, but more slowly. The distance between the two length scales l and L represents the tails of the distribution functions, which are illustrated by the new exponents μ_2 and ν_2. For infinite systems, this distance goes to infinity and it indicates the rate of "catastrophic events", which are quite important in natural self-organized critical phenomena.

The Abelian sandpile model is commonly used to illustrate self-organized critical phenomena. Our model is simple but in nature most self-organized critical phenomena occur in complex fractal media and as we have shown, their dynamics may be affected by the fractal dimension of the medium. Also, in some of these phenomena, catastrophic events such as avalanches and floods cause changes in the medium and its corresponding fractal dimension. For example, earthquakes change the fractality of a fault planes. These changes are taken to be a hysteresis effect in some models. For example, the effect of the history is considered in some earthquake models using faults [18]. In such cases, faults might be considered as fractal regions instead of simple curves [19–21]. To consider these cases, we used quenched fractal patterns with arbitrary dimensions. We violated the conservation of sand grains through the fractal patterns of the non-conservative sites and showed that the local violation of conservation does not destroy criticality in our model.

SOC has been demonstrated in the dynamics of many natural phenomena. Yet in many others, it remains hidden from us. The spatial fractal patterns produced as a result of SOC may surround other systems and as we have shown, contribute to the behavior of the tails of the distribution functions and the rate of catastrophic events in the surrounded systems. Thus, the activities of human beings (*i.e.*, industrialization) may cause a change in the fractality of these patterns. For example, deforestation changes the patterns of forests and deserts, thus changing the diversity of living organisms in these ecosystems. Today, it is common to illustrate climate change by reporting the trends in the averages of ecological parameters. However, we need to be more or less concerned with a change in the tail of the distribution function which may even cause a change in a chain of self-organized critical systems, since the high rate of catastrophic events causes damage to the ecosystem at a rate that might not be possible to be resolved before the next extreme event. Our argument could be summarized by a quote from Anderson [22], 'Much of the real world is controlled as much by the "tails" of distributions as by means or averages ...'

Acknowledgements The authors would like to express their gratitude to Dr. Bahman Farnudi for his assistance in editing this paper. We also thank Dr. Mostafa Mortazavifar for his contribution in developing the code for our first sandpile model, which is partially redeveloped to be used in the current research. This research was supported by the Institute for Advanced Studies in Basic Sciences (Grant No. G2018IASBS12644).

References

1. Bak, P., Tang, C., Wiesenfeld, K.: Self-organized criticality. Phys. Rev. A **38**(1), 364 (1988). https://doi.org/10.1103/PhysRevA.38.364
2. Bak, P.: How Nature Works: The Science of Self-organized Criticality. Springer, New York (1996)
3. Jensen, H.J.: Self-organized Criticality: Emergent Complex Behavior in Physical and Biological Systems, vol. 10. Cambridge Univ. Press, New York (1998)
4. Bak, P., Tang, C., Wiesenfeld, K.: Self-organized criticality: An explanation of the $1/f$ noise. Phys. Rev. Lett. **59**(4), 381 (1987). https://doi.org/10.1103/PhysRevLett.59.381

5. Dhar, D.: The Abelian sandpile and related models. Physica A **263**(1–4), 4 (1999). https://doi.org/10.1016/S0378-4371(98)00493-2
6. Manna, S., Kiss, L.B., Kertész, J.: Cascades and self-organized criticality. J. Stat. Phys. **61**(3), 923 (1990). https://doi.org/10.1007/BF01027312
7. Tsuchiya, T., Katori, M.: Proof of breaking of self-organized criticality in a nonconservative Abelian sandpile model. Phys. Rev. E **61**(2), 1183 (2000). https://doi.org/10.1103/PhysRevE.61.1183
8. Moghimi-Araghi, S., Sebtosheikh, M.: Annealed and quenched disorder in sand-pile models with local violation of conservation. Phys. Rev. E **92**(2), 022116 (2015). https://doi.org/10.1103/PhysRevE.92.022116
9. Daerden, F., Vanderzande, C.: Sandpiles on a Sierpinski gasket. Physica A **256**(3–4), 533 (1998). https://doi.org/10.1016/S0378-4371(98)00210-6
10. Falconer, K.: Fractal Geometry: Mathematical Foundations and Applications, 2nd edn. Wiley, West Sussex (2003)
11. Moghimi-Araghi, S., Mollabashi, A.: Chaos in sandpile models. Mod. Phys. Lett. B **25**(08), 569 (2011). https://doi.org/10.1142/S0217984911025900
12. Makse, H.A., Havlin, S., Schwartz, M., Stanley, H.E.: Method for generating long-range correlations for large systems. Phys. Rev. E **53**(5), 5445 (1996). https://doi.org/10.1103/PhysRevE.53.5445
13. Schneider, C.A., Rasband, W.S., Eliceiri, K.W.: NIH Image to ImageJ: 25 years of image analysis. Nat. Methods **9**(7), 671 (2012). https://doi.org/10.1038/nmeth.2089
14. Grassberger, P., Procaccia, I.: Measuring the strangeness of strange attractors. In: Hunt, B.R., Li, T.Y., Kennedy, J.A., Nusse, H.E. (eds.) The Theory of Chaotic Attractors, p. 170. Springer, New York (2004)
15. Lübeck, S., Usadel, K.D.: Numerical determination of the avalanche exponents of the Bak–Tang–Wiesenfeld model. Phys. Rev. E **55**(4), 4095 (1997). https://doi.org/10.1103/PhysRevE.55.4095
16. Moghimi-Araghi, S., Sebtosheikh, M.: The effect of the number of dissipative sites on a sandpile model. J. Phys. A **48**(8), 085001 (2015). https://doi.org/10.1088/1751-8113/48/8/085001
17. Bevington, P.R., Robinson, D.K.: Data Reduction and Error Analysis for the Physical Sciences, 3rd edn. McGraw-Hill, New York (2003)
18. Lippiello, E., de Arcangelis, L., Godano, C.: Memory in self-organized criticality. Europhys. Lett. **72**(4), 678 (2005). https://doi.org/10.1209/epl/i2005-10292-x
19. Ram, A., Roy, P.N.S.: Fractal dimensions of blocks using a box-counting technique for the 2001 Bhuj earthquake, Gujarat. India. Pure App. Geophys. **162**(3), 531 (2005). https://doi.org/10.1007/s00024-004-2620-4
20. Aki, K.: A Probabilistic Synthesis of Precursory Phenomena. In: Simpson, D.W., Richards, P.G. (eds.) Earthquake Prediction: An International Review. Maurice Ewing, vol. 4, pp. 566–574. American Geophysical Union, Washington, DC (1981)
21. Turcotte, D.L.: A fractal model for crustal deformation. Tectonophysics **132**(1–3), 261 (1986). https://doi.org/10.1016/0040-1951(86)90036-3
22. Anderson, P.W.: Some thoughts about distribution in economics. In: Arthur, W.B., Durlauf, S.N., Lane, D.A. (eds.) The Economy as an Evolving Complex System II, pp. 565–567. Addison-Wesley, Reading (1997)